

A Novel Melt-Based Route to Aluminium Foam Production

V. Gergely, T. W. Clyne

Department of Materials Science and Metallurgy, University of Cambridge,
Pembroke Street, Cambridge, CB2 3QZ, U.K.

Abstract

A novel melt processing technique is presented which combines some of the advantages of established melt- and powder-route approaches to metallic foam production. Production of the foam is a two-stage operation. In the first stage, a pretreated gas-generating powder (TiH_2) is dispersed into an aluminium/ SiC_p composite melt. A precursor material having a relatively low porosity is produced by allowing this melt to solidify. The powder pretreatment consists of a heat treatment sequence which generates a diffusion barrier (TiO_2) on the powder particle surface, which then prevents excessive hydrogen evolution during dispersion and subsequent casting. In the second stage of the operation, the precursor material is heated above the matrix melting point, when progressive evolution of hydrogen converts it into a cellular structure. Relationships between the processing parameters and the foam structure are explored.

1 Introduction

There are currently two basic approaches available to manufacture of closed-cell aluminium foams via a melt route. The first, a batch casting process, has been developed in Japan¹. The process involves addition of calcium into a stirred molten aluminium, generating dispersed solid particles to enhance the melt viscosity. In the next step, a titanium hydride powder is incorporated into the melt. A thermal decomposition of the hydride generates gas foaming the melt. The second, *continuous* foam-casting technique was patented by Alcan². A principle of the method is bubbling gas (usually air) into an aluminium alloy/silicon carbide composite melt generating a foam on the melt surface. The foam is carried out using a conveyor belt to solidify. Production of aluminium foam by Hydro Aluminium, Norway, is based on similar process³. Another way to manufacture closed-cell aluminium foams is baking of a powder route precursor material containing a foaming agent⁴⁻⁶. In the present work, a novel melt route to production of aluminium alloy based composite foam is described that combines some of the attributes of the above techniques.

2 Experimental procedures

2.1 Foam processing

In the first stage, a pre-treated gas-generating titanium hydride powder ($\sim 30 \mu\text{m}$ diam.) is mixed with Al-12Si powder ($\sim 150 \mu\text{m}$ diam.) in the weight ratio 1:4. The pre-treatment consists of two-step thermal oxidation sequence ($400^\circ\text{C}/24$ hours + $500^\circ\text{C}/1$ hour) in air, to build up a titanium dioxide diffusion barrier layer on its surface. The powder mixture is dispersed into a gradually cooled Al-9Si/ SiC_p composite (DuralcanTM) melt ($\sim 620^\circ\text{C}$) using conventional mechanical stirring (1200 rpm). The melt is stirred for one minute after the powder introduction. The amount of incorporated foaming agent (FA) is 1.5 wt% of the

Table 1: List of sample codes, precursor characteristics and foam baking parameters.

| Sample Code | Al-9wt%Si Matrix Precursor | | | Foam Baking Parameters | | |
|-------------|----------------------------|--------------|----------|---------------------------------------|-----------------------|---------------------------------|
| | SiC _p [vol.%] | Porosity [%] | Mass [g] | Heating Rate* [°C min ⁻¹] | T _{max} [°C] | Dwell at T _{max} [min] |
| F-17 | 10 | 22.4 | 23.0 | ~150 | 650 | 0 |
| F-18 | | | 22.9 | | 670 | 0 |
| F-30 | | | 23.0 | | 650 | 2 |
| F-14 | 20 | 14.3 | 26.0 | | 650 | 0 |
| F-3 | | | 26.2 | | 670 | 0 |
| F-36 | | | 25.7 | | 650 | 2 |
| F-23 | 10 | 22.4 | 18.1 | ~110 | 629 | 2 |
| F-21 | | | 16.8 | | | 5 |
| F-24 | | | 16.8 | | | 8 |
| F-34 | 20 | 14.3 | 15.6 | | | 5 |
| F-32 | | | 17.5 | | | 8 |
| F-33 | | | 16.4 | | | 16 |

*Heating rates were derived from the slopes (100-450 °C) of the corresponding thermal profiles.

composite mass (~1 kg). This procedure produces a material, having a relatively low porosity level (~14-23 %). In the second stage of the operation, the precursor material, placed in a graphite mould (30×30×45 mm³), is heated into the liquid state, when progressive evolution of hydrogen converts it into a cellular structure. A maximum expansion ratio of the precursor is predetermined by the volume of the graphite mould. However, the mould is not hermetically sealed and therefore the mass of the precursor material may not be conserved during some baking experiments, because the melt leakage through the gas escape vents. The baking is carried out in a conventional laboratory furnace. The temperature is recorded using a thermocouple located in the mould cavity. A study was made of the effect of the thermal history of baking and the level of silicon carbide particles in the composite on the foam porosity and structure. Summary of sample codes, the melt route precursor characteristics and foam baking parameters are listed in Table 1. A schematic of the proposed scale-up of the technique for industrial production of nearly net-shape metallic foam components is depicted in Fig. 1.

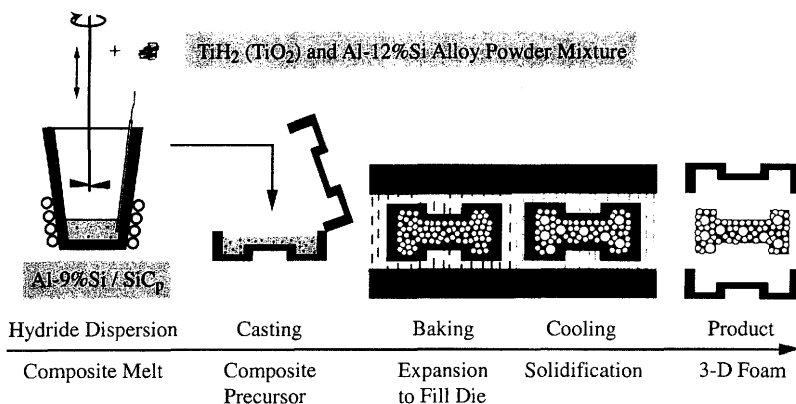


Fig. 1: Schematic of the proposed route for industrial production of nearly net-shape metallic foam components.

2.2 Foam structure characterisation

Image analysis has been carried out on vertical sections of the foam. The objective was to quantify the relationships between the processing parameters and the foam structure. The sections were obtained by cutting the foam using electrical discharge machining. Specimens were prepared as follows. Firstly, the surfaces were coated with black paint and exposed cells were filled with a transparent polyester casting resin. Secondly, the surfaces were polished to reveal the cell walls and edges. This procedure ensures that good contrast is achieved between the cell walls/edges and the black background and also eliminates cell wall rupture and smearing during specimen grinding. Finally, a digitised image (1200 dpi) of the surface of each specimen was obtained using a scanner. Image analysis was carried out using a KS 400 Imaging System, Release 3.0. The mean cell size is represented with a diameter (d) of a circle having an equivalent area to a corresponding cell-section. Pores smaller than 0.15 mm and those in the vicinity of the free surface of the casting were not included into the calculations.

3 Results and Discussion

3.1 Precursor preparation

A key requirement for effective preparation of the foamable precursor is that only a limited amount of hydrogen is released in the course the FA dispersion and subsequent solidification. The main factors which control this are: (1) The thickness of the titanium dioxide diffusion barrier layer on the FA surface, (2) The hydrogen concentration in the FA and (3) The initial melt temperature and subsequent cooling rate.

The beneficial effect of the surface oxide layer in slowing down the decomposition rate of the metal hydride during subsequent foam processing was first reported by Speed⁷. In accordance with his patent, a particulate FA has to be intimately admixed with discrete particles of material containing a major proportion of aluminium before the hydride thermal pre-oxidation treatment (454-482 °C/5-20 minutes). The proportion of decomposable material to aluminium-containing material is a critical aspect of the process. Gergely and Clyne⁸ showed that prior-mixing of the FA with an aluminium powder is not a necessary requirement for efficient pre-treatment of the FA. In the present work, a two stage treatment has been employed. Firstly, the powder was oxidised at 400 °C for 24 hours. A relatively thin surface oxide layer is reported⁹ to build up during oxidation of titanium at this temperature. However, this layer is sufficient to protect the sub-surface hydride against subsequent holding at 500 °C. The powder was periodically agitated during the pre-treatment in order to ensure uniform pre-oxidation. Thermogravimetric analysis of the oxidation process showed that, during a ramp to 500 °C and a dwell at this temperature, the oxidation kinetics are significantly accelerated. This results in formation of a thicker diffusion barrier layer, minimising the loss of the hydrogen in the FA during its incorporation into the composite melt. The effect of the titanium hydride pre-oxidation conditions on the onset temperature for significant hydrogen evolution (the onset of the powder mass loss) in the course of thermal treatment in argon is shown in Fig. 2. The heating rate of the powder was 20 °C min⁻¹. Two main points can be inferred from the thermogravimetric curves. (1) The onset of hydrogen evolution from the pre-treated hydride is postponed by several minutes in comparison with the as-received one, depending on the hydride pre-oxidation conditions. (2) The amount of released hydrogen (percentage of the mass loss) from the as-received hydride and the one oxidised for 24 h @ 400 °C is the same. This means that only a minimal amount of hydrogen is lost when the powder is pre-treated under these conditions.

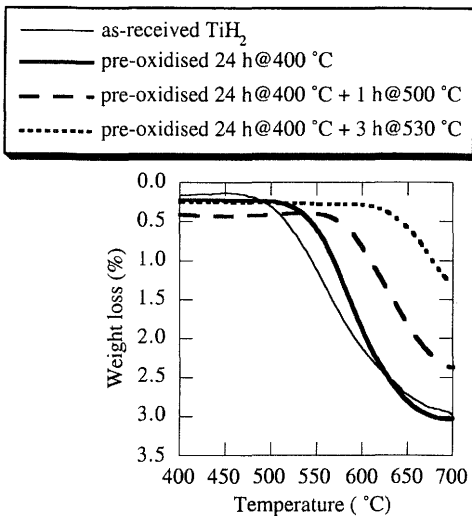


Fig. 2: Thermogravimetric curves for heating of as-received and pre-oxidised TiH_2 powder in argon, showing the effect of the powder pre-treatment on the delay before hydrogen evolution. The heating rate was $20^\circ\text{C min}^{-1}$.

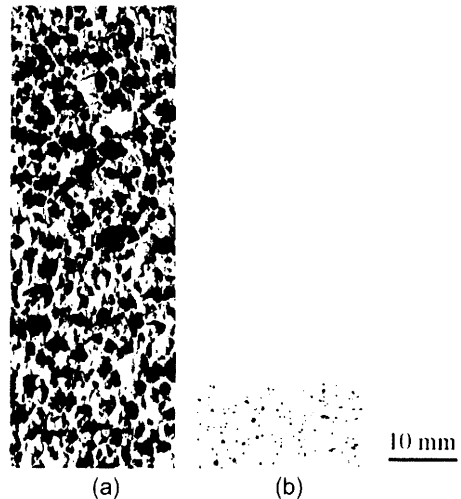


Fig. 3: Sections from Al-9Si/20 vol% SiC_p composites showing the effect of TiH_2 powder pre-treatment on casting porosity (P). Samples were produced under the same processing conditions and have an equal mass. (a) $P=84\%$, as-received TiH_2 powder; (b) $P=14.3\%$, TiH_2 powder pre-oxidised for 24 h @ 400°C + 1 h @ 500°C .

However, thermogravimetric curves recorded from powder pre-oxidised at 500°C or higher show that the weight loss is smaller. This indicates that some hydrogen is evolved during the powder pre-treatment.

Figs. 3 (a) and (b) show sections from Al-9Si/20 vol% SiC_p precursor material, demonstrating the effect of TiH_2 pre-treatment on casting porosity. A comparison of the porosity levels shows that pre-treatment of the FA can significantly delay the onset of hydrogen evolution. This is expected to occur, not only during the TGA experiments in argon, but also when the powder particles are surrounded by molten aluminium. The proposed route for foam production is based on this phenomenon.

3.2 Foam baking

The final structure of the foam is a result of interplay of three complex mechanisms: (1) bubble nucleation, (2) expansion of bubbles due to hydrogen evolution from a gas-generating hydride particle and (3) gas and semi-liquid material redistribution in the expanding and/or standing foam. In this section, experimental results are presented showing relationships between the processing parameters and the foam structure. Vertical cross-sections of the composite foams are shown in Figs. 4 (a)-(l). The volume percentage of silicon carbide particles in the composite material and the thermal parameters of the foam baking are listed in Table 1. Foam porosity levels and the mean cell sizes are given in the figure caption.

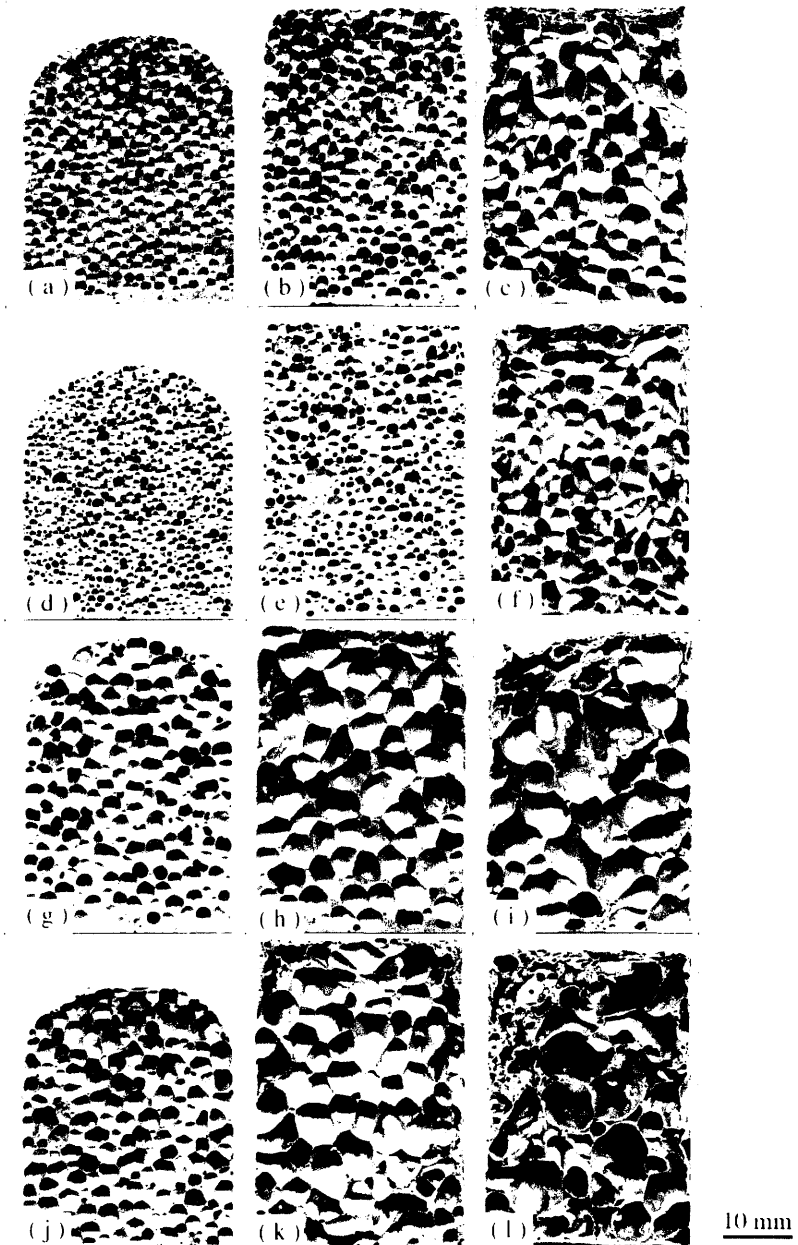


Fig. 4: Cross-sections of Al-9Si/SiCp composite foams showing the effect of melt viscosity (volume fraction of silicon carbide particles) and processing parameters on the foam macrostructure, porosity (P) and the mean cell size (d). List of sample codes, composite characteristics and foam processing parameters are given in Table 1. (a) F-17, $P \approx 69\%$, $d = 1.1$ mm; (b) F-18, $P \approx 74\%$, $d = 1.4$ mm; (c) F-30, $P \approx 89\%$, $d = 2.4$ mm; (d) F-14, $P \approx 58\%$, $d = 0.8$ mm; (e) F-3, $P \approx 73\%$, $d = 1.2$ mm; (f) F-36, $P \approx 82\%$, $d = 1.8$ mm; (g) F-23, $P \approx 79\%$, $d = 1.9$ mm; (h) F-21, $P \approx 88\%$, $d = 3.1$ mm; (i) F-24, $P \approx 90\%$, over-baked; (j) F-34, $P \approx 78\%$, $d = 1.6$ mm; (k) F-32, $P \approx 89\%$, $d = 2.4$ mm; (l) F-33, over-baked.

Several interesting trends are apparent. (1) Foams which contain higher amount of silicon carbide particles, baked under the same conditions as those containing a lower amount, generally show lower porosity levels and smaller cell sizes. (2) Higher baking temperatures and longer times result in production of foams with higher porosity levels and larger mean cell sizes. (3) The difference in mean cell size between foams containing 10 and 20 vol% of SiC_p becomes greater for foams baked at lower temperatures for longer times. (4) Structural degradation of the foam (Figs. 4 (i) and (l)) occurs when it is baked for a relatively long time in an enclosed mould. However, preliminary experiments not reported in detail here indicate that good structural stability is observed when the foams are allowed to expand freely in a vertical direction (without the constrained mould). There are thus three main factors which control the foam porosity and cell size demonstrated in Figs. 4 (a)-(l): (i) the amount and kinetics of hydrogen evolution, (ii) composite melt viscosity and (iii) critical cell wall thickness for rupture.

(i) Temperature-pressure-concentration (T-p-C) relationships for the Ti-H system have been recently evaluated by Wang¹⁰ and they are relatively well established. An examination of p-C isotherms of the system show that a rise of the system temperature from ~600 °C to ~700 °C increases the equilibrium hydrogen pressure over the system by one order of magnitude at a fixed concentration of hydrogen in titanium. Similarly, a change of H/Ti ratio from 1.9 to 1.7 drops the equilibrium pressure over the system at constant temperature (~606 °C) by one order of magnitude. These thermodynamic relationships indicate why a 20 °C difference in foam baking temperature significantly increases the foam porosity (see Figs. 4 (c) and (g)). Another implication of the relationships for foam processing is that adjusting the hydrogen concentration in the FA could offer some additional flexibility in control over the kinetics of hydrogen (precursor/foam porosity) evolution.

(ii) A necessity to enhance the melt viscosity for stabilisation of liquid metal foams is generally recognised^{1,2}. In practice, this is usually done by incorporation or generation of particles in the melt. They not only increase the bulk melt viscosity, but also increase the surface viscosity of cell walls and Plateau borders. A significant fraction of particles tend to be located at the gas/melt interface, slowing down the drainage processes. A theoretical analysis of the effect of viscosity on material redistribution in liquid metal foams is given elsewhere¹¹. The present experimental study shows that an increase in SiC_p fraction stabilises the foam for a longer period (see Figs. 4 (i) and (k)) and manipulation of the solid fraction can be used for production of "structurally identical" foams (cell size and porosity) using different thermal profiles of baking (see Figs. 4 (g) and (j)).

(iii) The limited scope for obtaining high porosity foams with small cell sizes is probably related to the fact that the critical cell wall thickness for rupture is relatively high for a composite foam system. This inhibits cell walls from becoming thin without cell coalescence occurring, which is a necessary requirement for fine cells. Microstructural examination of thin/ruptured cell walls has indicated¹² that the critical cell wall thickness is greater in the presence of ceramic particles. Simulations of capillary-driven cell wall thinning have shown¹³ that a moderate decrease in the size of the critical cell wall thickness can significantly slow down cell coarsening due to cell wall rupture. Moreover, a decrease in the size of the ceramic particles should lead to a higher number of particles at the same volume fraction concentration at the melt/gas interface. This further increases the cell wall/Plateau border surface viscosity and therefore the overall foam stability. Hence there is a strong incentive to use finer ceramic particles in the MMC material.

4 Conclusions

A novel melt-based route for metallic foam production is presented. It involves preparation of a precursor material by dispersion of gas-generating powder particles (pre-treated to delay gas release) in a liquid aluminium-based/SiCp composite, followed by solidification. Thermal decomposition of the foaming agent is induced by remelting the precursor within a die to generate foaming of the melt.

The process provides for flexibility in design of foam structures via relatively easy control over the amount/kinetics of hydrogen evolution and the drainage processes which occur during foam formation. This is facilitated by manipulating parameters such as the foaming agent pre-treatment, thermal histories during baking and composite melt viscosities (ceramic particle content and size).

Acknowledgements

One of the authors (VG) is thankful to the CVCP of UK universities for an Overseas Research Students Award and the Cambridge Overseas Trust for a scholarship. Additional funding was provided by the Department of Engineering through the Harvard MURI Prime Grant No. 00014-96-1-1028.

References

1. S. Akiyama, H. Ueno, K. Imagawa, A. Kitahara, S. Nagata, K. Morimoto, T. Nishikawa and M. Itoh, *Foamed Metal and Method of Producing Same*, U.S. Patent 4,713,277, (1987).
2. I. Jin, L. D. Kenny and H. Sang, *Stabilized Metal Foam Body*, U.S. Patent 5,112,697, (1992).
3. P. Åsholt, *Manufacturing of Aluminium Foams from PMMC Melts Material Characteristics and Typical Properties*, Proc. Metal Foams, Ed.: J. Banhart, Bremen, MIT Publishing Bremen, (1997), pp. 27-37.
4. B. C. Allen, M. W. Mote and A. M. Sabroff, *Method of Making Foamed Metal*, U.S. Patent 3,087,807, (1963).
5. J. Baumeister and H. Schrader, *Methods for Manufacturing Foamable Metal Bodies*, U.S. Patent 5,151,246, (1992).
6. F. Simancik and F. Schörghuber, *Complex-Shaped Foamed Aluminium Parts as Permanent Cores in Aluminium Castings*, Proc. Porous and Cellular Materials for Structural Applications, Eds.: D. S. Schwartz, D. S. Shih, A. G. Evans and H. N. G. Wadley, San Francisco, MRS, (1998), pp. 151-157.
7. S. E. Speed, *Foaming of Metal by the Catalyzed and Controlled Decomposition of Zirconium Hydride and Titanium Hydride*, U.S. Patent 3,981,720, (1976).
8. V. Gergely and T. W. Clyne, *The Effect of Oxide Layers on Gas-generating Hydride Particles during Production of Aluminium Foams*, Proc. Porous and Cellular Materials for Structural Applications, Eds.: D. S. Schwartz, D. S. Shih, A. G. Evans and H. N. G. Wadley, San Francisco, MRS, (1998), pp. 139-144.
9. T. Fukuzuka, K. Shimogori, H. Satoh and F. Kamikubo, *On the Beneficial Effect of the Titanium Oxide Film Formed by Thermal Oxidation*, Proc. 4th Int. Conf. Titanium, Eds.: H. Kimura and O. Izumi, Kyoto, AIMM and Petroleum Engineers, (1980), pp. 2783-2792.
10. W.-E. Wang, *Thermodynamic Evaluation of the Titanium-Hydrogen System*, J. Alloys Compounds, 238 (1996), pp. 6-12.
11. V. Gergely and T. W. Clyne, *Modelling of Material Redistribution During Melt Route Processing of Metallic Foams*, Euromat 99, Symp. MMCs and Metallic Foams, Munich, (1999), (abstract submitted).
12. V. Gergely and T. W. Clyne, *Acta Mater.*, (in preparation).
13. V. Gergely, F. Simancik, T.J. Matthams and T. W. Clyne, *Preparation of Ceramic/Metal Foam Laminates Using an In Situ Foaming Technique*, Proc. 12th Int. Conf. Composite Material, Ed.: T. Massard, Paris, (1999), (in print).